Metastable states of surface nanostructure arrays studied using a Fokker-Planck equation

T. P. Munt
Department of Physics, School of Engineering and Physical Sciences, Heriot-Watt University, Edinburgh EH14 4AS, United Kingdom

D. E. Jesson
School of Physics, Monash University, Victoria 3800, Australia

V. A. Shchukin* and D. Bimberg
Institut für Festkörperphysik, Technische Universität Berlin, D-10623 Berlin, Germany

(Received 18 September 2006; revised manuscript received 16 November 2006; published 13 February 2007)

We consider the coarsening of surface nanostructures which possess a minimum in formation energy per atom as a function of island size. The time evolution of the island size distribution function is evaluated using an approach based on a Fokker-Planck equation. Competition between chemical potential driven drift and thermal diffusive broadening of the island size distribution results in narrow Gaussian-like metastable states. The existence of these states, which allow the possibility of tuning the mean island size through the incorporation of a deposition flux, depends only upon the presence of a positive gradient in island chemical potential with respect to island size. Such behavior has important implications for the fabrication of uniformly sized quantum dot arrays with size selectivity.

DOI: 10.1103/PhysRevB.75.085422 PACS number(s): 81.07.Ta, 68.35.Md, 68.65.−k, 81.16.−c

I. INTRODUCTION

The self-assembly and self-organization of nanoscale structures on surfaces is of current interest as a means of fabricating novel devices, such as quantum dot lasers.[1,2] This is achieved by depositing heteroepitaxial films in the Stranski-Krastanow or Volmer-Weber growth mode by techniques such as molecular beam epitaxy.[3–9] Following their formation, surface islands (or dots) are subsequently overgrown by appropriate material layers to form the basis of quantum dot electronic, optical, or magnetic devices. For many applications, however, size uniformity of the dots is a critical issue which has led to appreciable efforts to understand the coarsening of quantum dot arrays.

Surface nanostructures which possess a minimum in the formation energy per atom (MEA) as a function of island size are particularly attractive candidates for device applications because the minimum corresponds to a thermodynamically favored size. By simply annealing such structures, one might anticipate the creation of arrays with good size uniformity. Theoretical studies have demonstrated that coherently strained two-dimensional (2D) islands,[10–13] three-dimensional (3D) islands with surface stress discontinuities at their edges,[14,15] or 3D islands with strain-renormalized surface energy[14,16] are all potential candidates for MEA systems. In the case of 2D strained islands, the discontinuity of the intrinsic surface stress tensor at the island edges contributes an elastic energy due to relaxation at the edges of the islands. Since this energy when expressed per atom exhibits a minimum as a function of island size, such islands are always MEA systems.[10–13] For 3D islands the minimum contributed by the discontinuity of the intrinsic surface stress tensor at the edges may lead to a minimum in the total island energy per atom as a function of island size, depending on the relative value of the surface energy change due to island formation. If the surface energy cost is not too large then a minimum will exist so that such islands are MEA systems.[14,15,17] In the case of 3D islands with strain-renormalized surface energy,[2,14,16] the surface energy cost of island formation can be substantially lowered by strain. In this case the minimum in the formation energy per atom is enhanced so that such islands are strong candidates for MEA systems. Whether a particular system is indeed an MEA system will depend in detail on step or facet energies, for example, which are in principle accessible by *ab initio* calculations. Although it is not possible to identify MEA characteristics *a priori*, a wide range of material systems may possess MEA energetics for certain growth temperatures and alloy compositions (e.g., strained semiconductor alloy 2D and 3D islands and quantum dots or metallic islands with surface stress discontinuities). It is therefore important to investigate how the minimum in formation energy per atom as a function of island size influences the coarsening behavior of MEA systems in order to best exploit this characteristic and obtain arrays with good size uniformity.

In this paper we will investigate the evolution of MEA systems of islands using an approach based on a Fokker-Planck equation. The feature arising from the analysis is the existence of dynamic metastable states which effectively prevent thermodynamic equilibrium being reached on experimentally relevant time scales. The existence of such states has been briefly reported in Ref. 18. Here we discuss the ripening of MEA systems in detail, emphasizing the features of MEA system metastability and contrasting with conventional capillarity-driven ripening. In particular, we outline the central approximations upon which the Fokker-Planck model of ripening is based.

II. A FOKKER-PLANCK EQUATION DESCRIPTION OF COARSENING

The use of a Fokker-Planck equation is a standard approach to describe time-dependent nucleation[19] and the

coarsening of surface nanostructures.[20] It can be derived as an approximation of the kinetic Becker-Döring equations for the aggregation of particles.[21] Here, our derivation will resemble the approach of Christian.[19]

Consider an array of surface islands or clusters at thermodynamic equilibrium. It follows from the principle of detailed balance that the number of islands that change (per unit area per unit time) their number of atoms from N to $N+1$ must equal the number of islands that change their number of atoms from $N+1$ to N. Here we neglect processes involving multiple attachments/detachments which are less probable. Therefore, if $W(N \rightarrow N+1)$ and $W(N+1 \rightarrow N)$ are the relevant transition rates, then

$$W(N \rightarrow N+1) f_{\mathrm{eq}}(N) = W(N+1 \rightarrow N) f_{\mathrm{eq}}(N+1), \quad (1)$$

where $f_{\mathrm{eq}}(N)$ is the equilibrium island size distribution function. The equilibrium distribution is given by the Gibbs-Boltzmann formula,

$$f_{\mathrm{eq}}(N) = \exp\left\{\frac{1}{k_{\mathrm{B}}T}[\bar{\mu}N - E(N)]\right\}, \quad (2)$$

where $E(N)$ is the energy of an island containing N atoms, $\bar{\mu}$ is the chemical potential of the system, and T is the absolute temperature. In the general case, when the island distribution is not at equilibrium, a flux $J(N,t)$ in the configurational space of island sizes occurs, given by the net transfer between islands containing N and $N+1$ atoms:

$$J(N,t) = W(N \rightarrow N+1) f(N,t) - W(N+1 \rightarrow N) f(N+1,t), \quad (3)$$

where t denotes time. The equilibrium relationship Eq. (1) may then be combined with Eq. (3) in the useful form,

$$J(N,t) = f_{\mathrm{eq}}(N) W(N \rightarrow N+1) \left[\frac{f(N,t)}{f_{\mathrm{eq}}(N)} - \frac{f(N+1,t)}{f_{\mathrm{eq}}(N+1)}\right]. \quad (4)$$

Provided the islands are not too small, we can regard N as a continuous variable and write Eq. (4) in the differential form:

$$J(N,t) = -f_{\mathrm{eq}}(N) W(N \rightarrow N+1) \frac{\partial}{\partial N}\left[\frac{f(N,t)}{f_{\mathrm{eq}}(N)}\right], \quad (5)$$

where the continuous island size distribution function $f(N,t)$ is defined such that $f(N,t)dN$ specifies the number of islands per unit area of the surface containing a number of atoms between N and $N+dN$ at time t. Substituting Eq. (2) into Eq. (5) then gives

$$J(N,t) = \omega(N)\left\{\frac{\bar{\mu} - \mu(N)}{k_{\mathrm{B}}T} f(N,t) - \frac{\partial}{\partial N} f(N,t)\right\}, \quad (6)$$

where $W(N \rightarrow N+1)$ has been written as $\omega(N)$ and $\mu(N)$ is the island chemical potential defined in terms of the continuous variable N by

$$\mu(N) = \frac{dE(N)}{dN}. \quad (7)$$

Finally, we note that the rate of change of the island size distribution is given by the continuity equation

$$\frac{\partial}{\partial t} f(N,t) = J(N-1,t) - J(N,t), \quad (8)$$

which can be written in terms of the continuous variable N as follows:

$$\frac{\partial}{\partial t} f(N,t) = -\frac{\partial}{\partial N} J(N,t). \quad (9)$$

Substituting Eq. (6) into Eq. (9) forms a Fokker-Planck equation for the time evolution of the island size distribution. This Fokker-Planck equation can be explicitly written in terms of two contributions:

$$\frac{\partial}{\partial t} f(N,t) = K_{\mathrm{drift}}(N,t) + K_{\mathrm{diff}}(N,t). \quad (10)$$

Here $K_{\mathrm{drift}}(N,t)$ is the drift contribution, given by

$$K_{\mathrm{drift}}(N,t) = -\frac{\partial}{\partial N} u(N,t) f(N,t), \quad (11)$$

where $u(N,t)$ is the associated drift velocity of the islands in the configurational space of island size, given by

$$u(N,t) = \omega(N)\left[\frac{\bar{\mu} - \mu(N)}{k_{\mathrm{B}}T}\right]. \quad (12)$$

$u(N,t)$ describes the drift contribution to the rate at which an island of a given size N changes its size with time. The term $K_{\mathrm{diff}}(N,t)$ in Eq. (10) is the diffusion contribution and is given by

$$K_{\mathrm{diff}}(N,t) = \frac{\partial}{\partial N}\omega(N)\frac{\partial}{\partial N} f(N,t). \quad (13)$$

$K_{\mathrm{diff}}(N,t)$ has its origin in thermally induced random forces (noise). It becomes important when $f(N,t)$ has a high curvature (narrow distribution) or when the temperature is high. If the curvature of $f(N,t)$ is large and negative at a particular N (such as at the maximum point of a narrow distribution), we see from Eqs. (13) and (10) that the diffusion contribution to $\partial f(N,t)/\partial t$ is negative so that $f(N,t)$ at that point is lowered. This will tend to reduce the magnitude of the curvature at this point and the effect of the diffusion term is to smooth out and broaden the distribution.

III. QUASI-STEADY-STATE CONDITIONS

The chemical potential $\bar{\mu}$ corresponds in our model to the mean-field chemical potential of the adatom sea via which islands exchange material during coarsening. Its time dependence is determined by mass conservation. The total number of atoms per unit surface area $\mathfrak{J}$ is given by the sum of the adatom concentration $\overline{f_{\mathrm{ad}}}$ and an integral over all atoms in the islands,

$$\mathfrak{J} = \overline{f_{\mathrm{ad}}} + \int_0^\infty f(N,t) N dN. \quad (14)$$

We assume here a typical situation where atoms are present mainly in the form of single adatoms or combined in islands

having a significant number of atoms each, thus neglecting dimers, trimers, etc. An external deposition flux Φ changes the total number of atoms per unit area:

$$\Phi = \frac{d\Im}{dt}, \tag{15}$$

where Φ is the deposition flux in atoms per unit area of the surface per unit time. Inserting Eq. (14) into Eq. (15) gives

$$\Phi = \frac{\partial \overline{f_{\mathrm{ad}}}}{\partial t} + \int_0^\infty \frac{\partial f(N,t)}{\partial t} N dN. \tag{16}$$

Expressing the time derivative of the island size distribution function in terms of the island flux $J(N,t)$ from Eq. (9) and substituting this into Eq. (16) one obtains

$$\Phi = \frac{\partial \overline{f_{\mathrm{ad}}}}{\partial t} - \int_0^\infty \frac{\partial J(N,t)}{\partial N} N dN. \tag{17}$$

Integration of Eq. (17) by parts then yields

$$\Phi = \frac{\partial \overline{f_{\mathrm{ad}}}}{\partial t} - [NJ(N,t)]_{N=0}^{N=\infty} + \int_0^\infty J(N,t) dN. \tag{18}$$

The off-integral term in Eq. (18) can be shown to be negligible. Invoking the quasi-steady-state approximation[22] that the rate of change of the adatom concentration due to deposition balances the rate of change of the adatom concentration due to incorporation at growing islands, one can set $\partial \overline{f_{\mathrm{ad}}}/\partial t = 0$ yielding

$$\Phi = \int_0^\infty J(N,t) dN. \tag{19}$$

Then the flux in the configurational space of island size $J(N,t)$ integrated over all islands is equal to the deposition flux, i.e., the net total rate of change of the number of atoms in all islands is equal to the rate of deposition of atoms onto the surface. Note that by invoking the quasi-steady-state approximation in obtaining Eq. (19), we focus on the stage of growth after nucleation has completed.

Equation (19) is used to determine the time-dependent value of $\bar{\mu}$. Using Eqs. (10)–(13) and (19) we are able to model the evolution kinetics of $f(N,t)$ from an arbitrary initial distribution for a given Φ. Equation (10) is solved numerically and $\bar{\mu}$ updated after each time step using Eq. (19). We calculate the drift term given by Eq. (11) using the two-step Lax-Wendroff method[22,23] and Barton's method.[22,24] For the diffusion term given by Eq. (13) we use the forward time centered space method.[23] The time increment at each step in the computation is chosen small enough to simultaneously satisfy the stability criteria for both the drift and diffusion terms.

IV. TWO-DIMENSIONAL STRAINED ISLAND MODEL

To investigate the coarsening behavior of MEA systems we focus on a system of 2D strained islands of monolayer height which is the simplest system of this type. Such an array can be created during the early stages of Stranski-Krastanow growth by the deposition of a material onto a substrate which possesses a different lattice constant. We assume that the supersaturation and coverage are sufficiently low so that nucleation on top of the 2D islands can be neglected and that the array is sufficiently sparse so that elastic interactions between islands are negligible.[25] The formation energy of a single 2D island consisting of N atoms is then given by (Refs. 18 and 26–29)

$$E(N) = -WN + C_1\sqrt{N} - C_2\sqrt{N}\ln(\sqrt{N}). \tag{20}$$

Here the first term is the binding energy between atoms in the island. The second term is the energy of the island edges due to broken chemical bonds, where the constant C_1 is proportional to the energy of the edges normalized per one edge atom. The third term is the elastic relaxation energy associated with the discontinuity of the surface stress tensor at the island edges,[11,12] where the constant C_2 is proportional to the square of the lattice mismatch strain between the deposited material and the substrate.[28]

The relevant quantity to consider in determining the thermodynamic stability of an array of islands is the island energy per atom $\varepsilon(N) = E(N)/N$, rather than the energy per island $E(N)$. Minimizing $\varepsilon(N)$ is equivalent to minimizing the total energy of the array under the constraint of a fixed total amount of material in all islands.[30] Then the optimum distribution of material between individual islands is found.

The energy per atom $\varepsilon(N)$ always has a minimum at the optimum size (Ref. 12)

$$N_0 = \exp\left[2\left(\frac{C_1}{C_2} + 1\right)\right], \tag{21}$$

corresponding to the size at which islands are predicted to be thermodynamically stable.[31] At this size, the energy per atom is lower than in a very large island ($N \to \infty$) by the quantity $\varepsilon_0 = C_2 N_0^{-1/2}$. The quantities N_0 and ε_0 provide a characteristic scale to the island size and energy per atom, respectively. Expressing $\varepsilon(N)$ in these units gives

$$\frac{\varepsilon(N)}{\varepsilon_0} = -\frac{W}{\varepsilon_0} - \left(\frac{N}{N_0}\right)^{-1/2}\left[1 + \ln\left(\sqrt{\frac{N}{N_0}}\right)\right]. \tag{22}$$

The size-dependent part of $\varepsilon(N)/\varepsilon_0$ depends only on the dimensionless island size N/N_0, with no free parameters, and is plotted in Fig. 1(a).

To model the kinetics of island evolution, we require the chemical potential of an island, which is given by Eq. (7). Using Eq. (20) for $E(N)$ and expressing in the units ε_0 and N_0, Eq. (7) gives

$$\frac{\mu(N)}{\varepsilon_0} = -\frac{W}{\varepsilon_0} - \left(\frac{N}{N_0}\right)^{-1/2}\left[1 + \frac{1}{2}\ln\left(\sqrt{\frac{N}{N_0}}\right)\right]. \tag{23}$$

As for $\varepsilon(N)$ in Eq. (22), we see that in these units the size-dependent part of $\mu(N)$ depends only on N/N_0. $\mu(N)$ is displayed in Fig. 1(b) and has a minimum at $N_1 = N_0/e^2 \approx 0.14N_0$. Note the qualitative similarity of the variation with N when compared with $\varepsilon(N)$ in Fig. 1(a). We have set $W = 0$ in both Figs. 1(a) and 1(b) since the only effect of W is to produce a vertical shift in the curves, which will have no

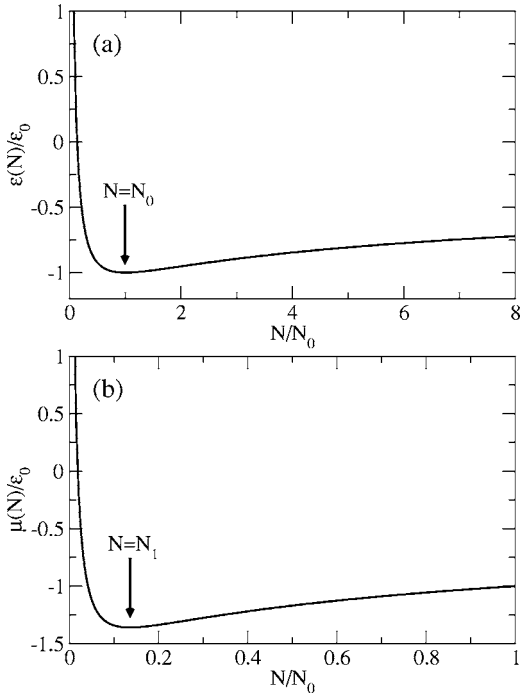

FIG. 1. (a) Energy per atom $\varepsilon(N)$ and (b) chemical potential $\mu(N)$ plotted as a function of N/N_0 for $W=0$. Minima in $\varepsilon(N)$ and $\mu(N)$ occur at $N=N_0$ and $N=N_1\approx 0.14N_0$, respectively.

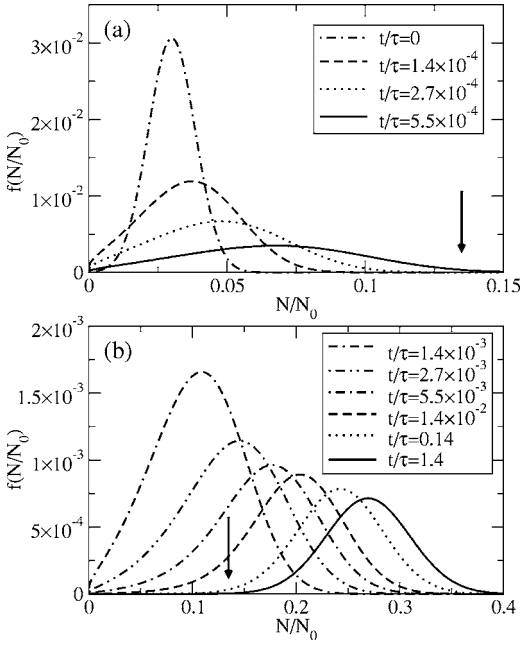

FIG. 2. (a) Early and (b) late evolution of $f(N,t)$ with time t upon annealing at the temperature $T/\Theta=10^{-3}$ for a Gaussian initial distribution located below N_1. The solid arrows indicate the chemical potential minimum at N_1.

effect upon the results of kinetic simulations. The presence of the minima in $\varepsilon(N)$ and $\mu(N)$ contrasts with the monotonically decreasing nature of these quantities with island size in conventional capillarity-driven ripening.

In modeling island evolution we assume a standard case where the kinetics is limited by attachment (detachment) processes of adatoms to (from) the island perimeter.[32–34] Then the kinetic factor $\omega(N)$ entering Eqs. (6), (12), and (13) is given by $\omega(N)=\xi N^{1/2}$ for 2D islands,[35] where $\xi(T)$ is a temperature-dependent kinetic rate.

V. SIMULATED ANNEALING OF MEA SYSTEMS

In this section we examine how MEA system energetics, as encapsulated in Fig. 1, influence the dynamical evolution of island arrays during annealing. We partition the discussion into two parts, with an initial island distribution located at sizes above and below the minimum in island chemical potential, respectively. This clarifies the origin and properties of metastable states which are the new feature of MEA dynamics. In particular, we highlight the link between the island array evolution and the salient features of the chemical potential behavior in Fig. 1(b).

We adopt the convention of measuring the temperature T with respect to the temperature $\Theta=C_2\sqrt{N_0}/k_B$ corresponding to the energy of an island containing N_0 atoms of energy per atom ε_0.[26] In all the simulation results which follow in this section we use the representative temperature $T/\Theta=10^{-3}$.

A. Initial size distribution below N_1

Consider the evolution of an array of islands with a Gaussian initial size distribution centered on a size significantly below the minimum in $\mu(N)$ at N_1. Figure 2 shows this initial distribution at $t/\tau=0$ and the subsequent early [Fig. 2(a)] and late [Fig. 2(b)] time evolution upon annealing. In Fig. 3 we plot the corresponding values of the terms $K_{\text{drift}}(N,t)$ and $K_{\text{diff}}(N,t)$ at selected times to assess the con-

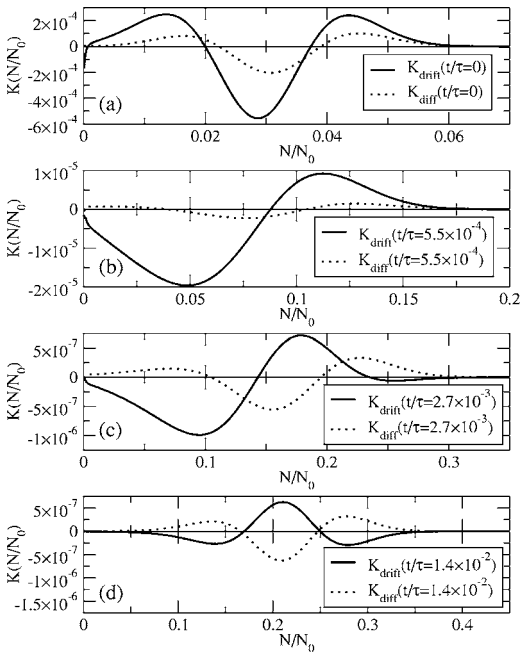

FIG. 3. Evolution of the terms $K_{\text{drift}}(N,t)$ and $K_{\text{diff}}(N,t)$ with time t corresponding to the results of Fig. 2. Parts (a)–(d) correspond to successively greater values of t.

tribution of each of these terms to the evolution. We adopt the convention of measuring the time t in the units $\tau = N_0^{3/2}/\xi$.

We see from Fig. 3(a) that at $t/\tau=0$ the term $K_{\text{drift}}(N,t)$ has a magnitude approximately three times that of the term $K_{\text{diff}}(N,t)$, hence the main contribution to the initial evolution is from the drift term. The early time evolution in Fig. 2(a) is therefore mainly driven by the negative gradient in chemical potential with respect to island size and, as such, is similar to conventional capillarity-driven ripening, in which the chemical potential decreases monotonically. In a drift-dominant regime with $\Phi=0$, Eq. (19) results in an expression for $\bar{\mu}$ which is a weighted mean of $\mu(N)$ over the size distribution, where the weighting is by $\omega(N)$. Small islands, with a chemical potential above $\bar{\mu}$, shrink [according to Eq. (12)] and large islands, with a chemical potential below $\bar{\mu}$, grow. The island size distribution therefore broadens and evolves to larger sizes as shown in Fig. 2(a). The diffusion term also contributes to this broadening, although its contribution during the early stages of evolution decreases so that by $t/\tau=5.5\times10^{-4}$, the magnitude of $K_{\text{diff}}(N,t)$ is only about one ninth that of $K_{\text{drift}}(N,t)$ [Fig. 3(b)].

At later time in Fig. 2(b), the distribution reaches and, surprisingly, passes slightly above N_1. As the distribution passes through N_1, the drift and diffusion terms become closer in magnitude. By $t/\tau=1.4\times10^{-2}$, the two terms have evolved into a balance, becoming almost equal in magnitude but opposite in sign [see Fig. 3(d)]. This results in a cancellation of the terms to one part in nine, hence the rate of evolution of the array slows significantly. Above N_1, the distribution narrows slightly and the two terms continue to become closer in magnitude, slowing the evolution further. By $t/\tau=1.4$, the terms cancel to one part in 2.4×10^3. Note the exponential decrease in the rate of evolution of $f(N,t)$ with time in the later stages of Fig. 2(b). It is expected that the evolution will continue to slow and become negligible beyond this point. The cancellation of the drift and diffusion terms produces a metastable state which effectively suppresses the evolution of $f(N,t)$ on experimentally relevant time scales.

By $t/\tau=1.4$, essentially the whole distribution lies above N_1. This contrasts with the conventional view that the evolution stops at the chemical potential minimum.[15,36] Note that passing through the minimum is a consequence of the drift term and occurs even in the absence of the diffusion term. Therefore, the minimum in chemical potential does not formally determine an optimum island size, even in the drift-dominated regime. If features are included which promote additional island size uniformity, such as island migration in the presence of elastic interactions,[36] then the distribution may be very narrow when approaching N_1. In this case, the narrow width may mean that the extent to which N_1 is exceeded when the metastable state is reached is small, although still finite.

B. Origin of metastability in terms of island dissolution rate

To further explain the drastic slowing of the island size distribution evolution and the onset of metastability in Fig. 2(b), consider the evolution of the number of islands in the array as a function of time. The mean number of atoms $\bar{N}$ per 2D island is given by

$$\bar{N} = q/n_{\text{isl}}, \tag{24}$$

where q is the surface coverage (the fraction of the surface covered by islands) and n_{isl} is the total concentration of islands per unit atomic site. Since the coverage q is conserved for 2D islands under zero deposition flux, any variation in $\bar{N}$ must be accompanied by a change in n_{isl}. So the growth of the overall distribution is limited by the magnitude of the variation in n_{isl} (although a narrowing/broadening of the distribution at fixed $\bar{N}$ could occur with constant n_{isl}). The rate of change of n_{isl} is given by the rate of dissolution of islands at the origin (Ref. 22)

$$\frac{dn_{\text{isl}}}{dt} = \lim_{N\to 0}[J(N,t)]. \tag{25}$$

Hence the rate of decrease of the total concentration of islands equals the flux of islands approaching zero size.

In conventional capillarity-driven ripening, where $\mu(N)$ decreases monotonically, the flux toward zero size is always significant. All islands with a size below that corresponding to the mean-field chemical potential $\bar{\mu}$ possess a chemical potential $\mu(N)>\bar{\mu}$ and therefore shrink toward the origin [via Eq. (12)]. Hence n_{isl} decreases via Eq. (25) and so $\bar{N}$ must increase. This continues until ultimately all atoms are collected into a single huge island.

For the 2D strained island chemical potential considered here, the situation is initially similar to that for conventional capillarity-driven ripening [Fig. 2(a)]. However, once the main body of the size distribution has passed above N_1 in Fig. 1(b), only a very limited number of islands will have a small enough size to give a chemical potential exceeding $\bar{\mu}$ (for the purpose of the present argument, it is helpful to consider the drift term in isolation). Hence only a very small number of islands, located in the tail of the distribution toward the origin, will be shrinking toward zero size. This number will decrease even further with time as islands in the tail are depleted as they go to zero size and dissolve, and also as $\bar{N}$ grows, which increases $\bar{\mu}$. So at late time, n_{isl} decreases very slowly and $\bar{N}$ can grow only very slowly, and these rates tend to zero. The distribution $f(N,t)$ therefore enters a metastable state with fixed $\bar{N}$.

The above argument is clear when considering the drift term in isolation. The diffusion term will also contribute to the flux toward zero size since $f(N,t)$ decreases toward the origin [hence the second term in the brackets of Eq. (6) contributes a negative flux]. However, this will only influence the precise point of balance below which size the islands shrink toward the origin, and will not affect our argument. At late time, the flux due to diffusion in the direction of the origin of the islands of size above N_1 is balanced by the drift

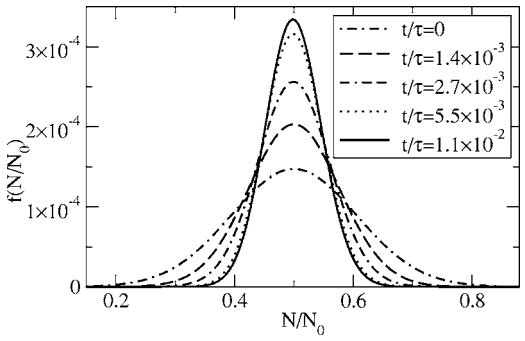

FIG. 4. Evolution of $f(N,t)$ with time t upon annealing at the temperature $T/\Theta=10^{-3}$ for a Gaussian initial distribution located above $N_1 \approx 0.14N_0$. A metastable state is reached by $t/\tau=1.1\times10^{-2}$.

term. Our simulations support the view that there are no islands remaining below N_1 once the metastable state is reached, these islands having either shrunk and completely dissolved, or grown and entered the main distribution.

C. Initial size distribution above N_1

We now further investigate the evolution of an array located on the positive chemical potential slope at sizes above N_1. In Fig. 4 we plot the evolution upon annealing of a Gaussian initial distribution located significantly above N_1. The distribution narrows, almost symmetrically, and stabilizes about the mean island size.

We can explain the observed evolution by considering the contribution of the drift and diffusion terms, which are plotted at the times $t/\tau=0$ and $t/\tau=1.1\times10^{-2}$ in Fig. 5. At $t/\tau=0$ in Fig. 5(a), the term $K_{\text{drift}}(N,t)$ has a magnitude approximately five times that of the term $K_{\text{diff}}(N,t)$, hence the main contribution to the initial evolution is from the drift term. Since $\mu(N)$ has a positive gradient in this regime, the islands undergo inverse ripening: small islands, with a chemical potential below $\bar{\mu}$, grow and large islands, with a chemical potential above $\bar{\mu}$, shrink.[37] Therefore the drift term causes the distribution to narrow about the mean island size, the opposite behavior to the broadening which would be observed in conventional capillarity-driven ripening. However, this narrowing is opposed by the diffusion term which increases with the curvature of the distribution and always produces a broadening effect. So as the distribution narrows due to the drift term, the contribution of the diffusion term increases. By $t/\tau=1.1\times10^{-2}$, the terms $K_{\text{drift}}(N,t)$ and $K_{\text{diff}}(N,t)$ have evolved into a balance [Fig. 5(b)], becoming very nearly equal in magnitude but opposite in sign. The terms almost completely cancel and the evolution becomes negligible,[38] resulting in array metastability.

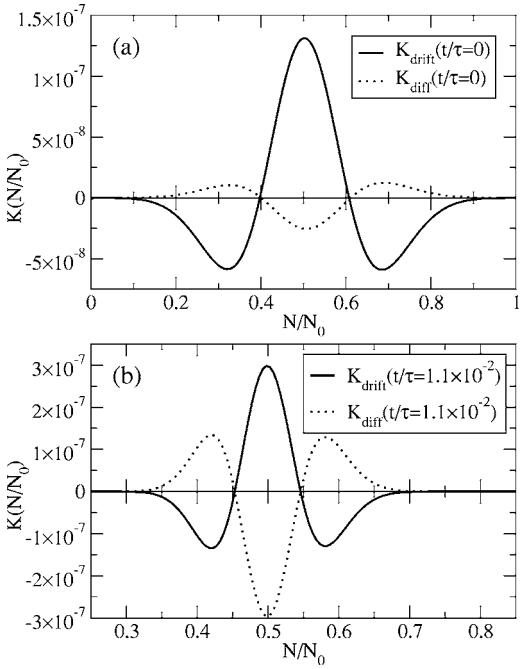

FIG. 5. Comparison of the terms $K_{\text{drift}}(N,t)$ and $K_{\text{diff}}(N,t)$ at (a) $t/\tau=0$ and (b) $t/\tau=1.1\times10^{-2}$, corresponding to the results of Fig. 4.

Note that because, from the outset, the whole distribution lies above N_1 and is narrowing, there is no flux of islands toward the origin. Then from Eq. (25) the number of islands n_{isl} is conserved. Hence from Eq. (24) we see that the array is constrained to evolve with constant $\bar{N}$. This is consistent with our observation of the narrowing of the size distribution around the mean island size observed in Fig. 4. Note also that the metastable state in Fig. 4 is reached much more rapidly than such a state is approached in Fig. 2. This is because in the latter case, the tail of the distribution toward the origin contributes to the evolution of $\bar{N}$ over a long time scale, as this population gradually decays and dissolves. The absence of such a population in the simulation of Fig. 4 explains the rapid onset of metastability in this case.

VI. PROPERTIES OF METASTABLE STATES

We saw in Secs. V A and V C how the island size distribution evolves to a metastable state which possesses the striking feature of a Gaussian shape. It is important to understand the factors which determine the width of the metastable size distribution with a view to controlling size distributions in MEA systems.

In this section we analyze the shape and form of the size distribution in a metastable state using an analytical approach within a linear chemical potential approximation.[18,29] This provides a direct explanation for the shape of the distribution and identifies the key factors determining the width of the distribution. We show that the analytical distribution width gives good agreement with the observed metastable distribution widths obtained from simulations at various temperatures.

A. Analytical description of metastability in the linear chemical potential approximation

The metastable states which we have numerically demonstrated are associated with the positive gradient in chemical

potential with island size for sizes $N > N_1$. If the size distribution is relatively narrow, then the variation of $\mu(N)$ with size N can be well approximated by a straight line with positive gradient over the width of the distribution. We consider the zero deposition case with a distribution located at a size such that the mean-field chemical potential $\bar{\mu} = \mu(N_m)$. Then within our approximation the island chemical potential at size N can be written

$$\mu(N) = \mu(N_m) + (N - N_m) \left. \frac{d\mu}{dN} \right|_{N=N_m}. \quad (26)$$

This linear form is inserted into Eq. (6) for the flux in size space $J(N,t)$ and steady-state solutions sought satisfying $J(N,t)=0$. This yields a metastable Gaussian centered on N_m:

$$f_m(N) = A_m \exp\left[- \frac{(N - N_m)^2}{2k_B T} \left. \frac{d\mu}{dN} \right|_{N=N_m} \right], \quad (27)$$

where A_m is a constant. Hence we see that N_m is identified with the mean island size $N_m = \bar{N}$. Thus $\bar{\mu} = \mu(\bar{N})$ which is consistent with the value obtained for $\bar{\mu}$ by using $f_m(N)$ in Eq. (19) with $\Phi = 0$.

The standard deviation of $f_m(N)$ is given by

$$\sigma(N_m) = \left[\frac{k_B T}{d\mu/dN|_{N=N_m}} \right]^{1/2}. \quad (28)$$

The full width at half maximum (FWHM) is then given by $\Delta_{anal}(N_m) = 2\sqrt{2 \ln 2}\,\sigma(N_m)$, which we present here in our preferred measurement units:

$$\frac{\Delta_{anal}(N_m)}{N_0} = 2\sqrt{2 \ln 2} \left[\frac{T/\Theta}{(d\mu/dN|_{N=N_m})/(\varepsilon_0/N_0)} \right]^{1/2}. \quad (29)$$

This gives an analytical expression for the predicted distribution width in a metastable state centered at N_m.

The chemical potential gradient is found by differentiating $\mu(N)$ in Eq. (23):

$$\frac{d\mu(N)/dN}{\varepsilon_0/N_0} = \frac{1}{8} \left(\frac{N}{N_0} \right)^{-3/2} \left[2 + \ln\left(\frac{N}{N_0} \right) \right]. \quad (30)$$

In Fig. 6 we plot $d\mu(N)/dN$ as a function of island size N. This attains its maximum value at $N_2 = e^{-4/3} N_0 \approx 0.26 N_0$. We expect a distribution centered at N_2 to display the narrowest

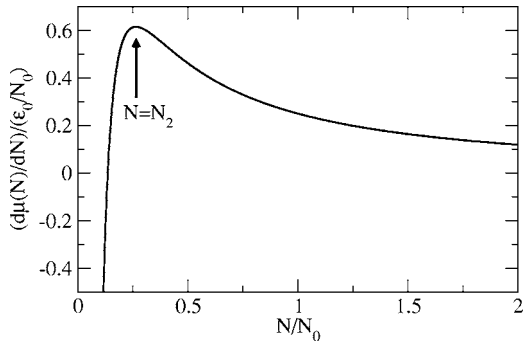

FIG. 6. Gradient of island chemical potential $d\mu(N)/dN$ plotted as a function of island size N. A maximum in $d\mu(N)/dN$ occurs at $N = N_2 \approx 0.26 N_0$.

width, with the width increasing for distributions centered at smaller or larger sizes. The approximation of a linear chemical potential variation will be most accurate close to N_2 (for sufficiently narrow distributions, i.e., low temperatures) or at very large island sizes, when $d\mu(N)/dN$ is approximately constant. However, at very large island sizes, the small magnitude of $d\mu(N)/dN$ will result in a large distribution width via Eq. (29), so that the variation in chemical potential gradient across the distribution in this case may still be significant enough to offset any increase in precision of the linear approximation. Note that the analytical results will not be valid if the distribution lies at sizes small enough that $d\mu(N)/dN$ is close to zero ($\bar{N} \to N_1$) or negative, when Δ_{anal} in Eq. (29) diverges or becomes undefined, respectively. In these cases, part of the distribution will lie below the chemical potential minimum at N_1 so that a shift in $\bar{N}$ is expected before metastability is attained (see Sec. V B).

It is possible to determine the normalization factor A_m of the metastable Gaussian in Eq. (27) by the mass conservation requirement that the number of atoms deposited is equal to the total number of atoms within the islands:

$$q = \int_0^\infty N f_m(N) dN, \quad (31)$$

where q is the surface coverage. Here $f_m(N)dN$ has been defined as the concentration of islands per unit atomic site containing a number of atoms between N and $N+dN$. Substituting Eq. (27) into Eq. (31) gives the following analytical expression for the normalization factor:

$$A_m^{anal}(N_m) = \frac{q}{\sigma^2 \exp\left[-\frac{1}{2}\left(\frac{N_m}{\sigma} \right)^2 \right] + \sqrt{\frac{\pi}{2}} N_m \sigma \left(1 - \mathrm{erf}\left[-\frac{1}{\sqrt{2}} \frac{N_m}{\sigma} \right] \right)}, \quad (32)$$

where σ is given by Eq. (28). This gives the peak height of the metastable distribution $f_m(N)$.

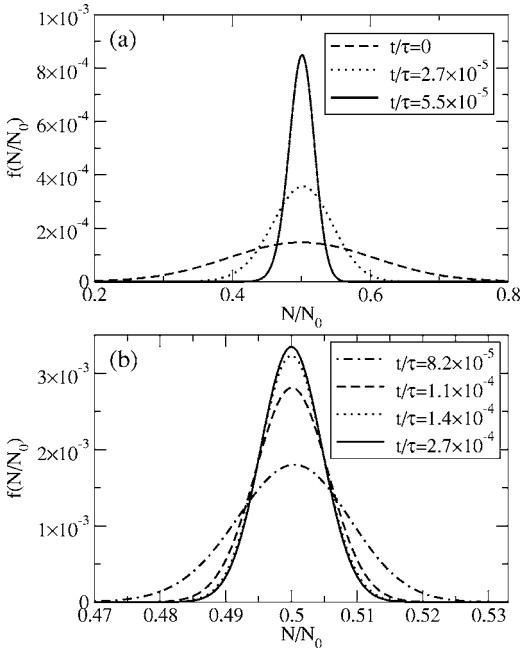

FIG. 7. (a) Early and (b) later evolution of $f(N,t)$ with time t upon annealing at the temperature $T/\Theta=10^{-5}$ for a Gaussian initial distribution located above N_1. A metastable state is reached by $t/\tau=2.7\times10^{-4}$. The initial distribution at $t/\tau=0$ is the same as that in Fig. 4.

B. Island size distribution widths

The metastable size distribution width obtained analytically in Eq. (29) indicates that narrower distributions are expected at lower temperatures or for steeper gradients in chemical potential. This allows the possibility of tuning the distribution width through varying the temperature or the material parameters. Changing the latter will alter the chemical potential gradient. For example, changing the lattice misfit strain would enable the manipulation of C_2, which is proportional to the square of the strain.

To investigate the temperature dependence of the size distribution width in a metastable state and test the validity of the analytical expression Eq. (29), we have performed array evolution simulations at different temperatures. From these simulations we obtain the metastable distributions numerically without the approximation of a linear chemical potential employed in Sec. VI A, which allows us to determine the accuracy of this approximation.

We extend the annealing simulation of Sec. V C for evolution above N_1 to various different temperatures T. Recall that the simulation in Sec. V C was performed at $T/\Theta=10^{-3}$ from a Gaussian initial distribution located significantly above N_1 (Fig. 4).

In Figs. 7 and 8 we repeat this simulation from the same Gaussian initial distribution for the temperatures $T/\Theta=10^{-5}$ and $T/\Theta=10^{-4}$, respectively. These are below the original temperature $T/\Theta=10^{-3}$ used in Fig. 4. As before, we observe almost symmetrical narrowing before metastable states are reached. However, at these lower temperatures, the diffusion term makes a smaller contribution so that the distribution narrows further before the magnitude of the diffusion term

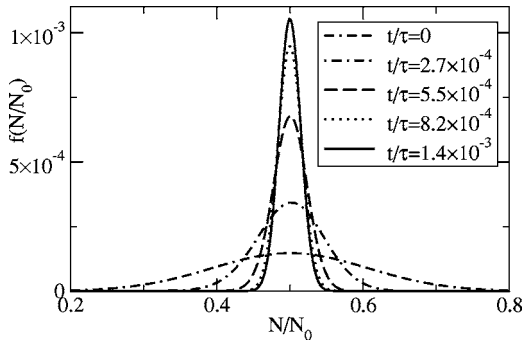

FIG. 8. Evolution of $f(N,t)$ with time t upon annealing at the temperature $T/\Theta=10^{-4}$ for a Gaussian initial distribution located above N_1. A metastable state is reached by $t/\tau=1.4\times10^{-3}$. The initial distribution at $t/\tau=0$ is the same as that in Fig. 4.

increases sufficiently to balance the drift term. Hence the narrowest width results for the lowest temperature $T/\Theta=10^{-5}$. Figure 9 shows simulation results for the higher temperature $T/\Theta=7.5\times10^{-3}$, which indicates that a broader metastable distribution results due to the larger contribution of the diffusion term.

Note that the units τ in which the time t is presented in Figs. 4 and 7–9 are not the same. The units τ depend on the temperature because the kinetic rate ξ entering the expression for τ is temperature dependent.

We now compare the widths of the metastable size distributions obtained numerically at different temperatures with the predicted widths obtained analytically within the linear chemical potential approximation of Sec. VI A. Table I makes a detailed comparison between these distribution widths, for the cases simulated above and in Sec. V C. It can be seen that the numerical and analytical widths agree in all cases to within 1%. Hence the approximation of a linear chemical potential variation leads to a remarkably good prediction of the size distribution in a metastable state. This demonstrates the validity of Eq. (29) in determining the metastable distribution width for a given temperature and mean island size.

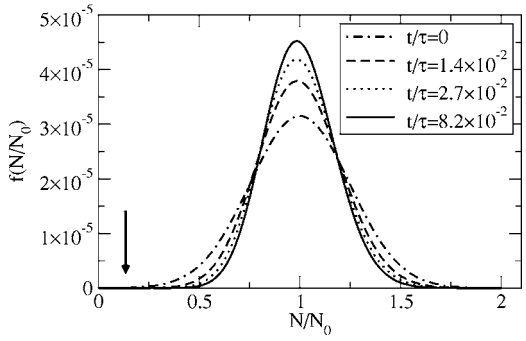

FIG. 9. Evolution of $f(N,t)$ with time t upon annealing at the temperature $T/\Theta=7.5\times10^{-3}$ for a Gaussian initial distribution located above N_1. A metastable state is reached by $t/\tau=8.2\times10^{-2}$. The initial distribution at $t/\tau=0$ is different from that in Fig. 4. The solid arrow indicates the chemical potential minimum at N_1.

TABLE I. Comparison of island size distribution widths in a metastable state. The full width at half maximum (FWHM) Δ_{num} corresponds to the metastable states reached numerically in Figs. 7(b), 8, 4, and 9 for the temperatures $T/\Theta=10^{-5}$, $T/\Theta=10^{-4}$, $T/\Theta=10^{-3}$, and $T/\Theta=7.5\times10^{-3}$, respectively. The FWHM Δ_{anal} corresponds to the analytical results obtained using Eq. (29).

T/Θ	$\bar{N}/N_0$	$\frac{d\mu/dN\|_{N=\bar{N}}}{\varepsilon_0/N_0}$	Δ_{num}/N_0	$\Delta_{anal}(\bar{N})/N_0$
10^{-5}	0.5	0.462	1.10×10^{-2}	1.10×10^{-2}
10^{-4}	0.5	0.462	3.47×10^{-2}	3.46×10^{-2}
10^{-3}	0.5	0.462	0.110	0.110
7.5×10^{-3}	1	0.250	0.405	0.408

VII. COMPARISON WITH THERMODYNAMIC EQUILIBRIUM

We have shown that the metastable states demonstrated in this paper arise through the dynamic cancellation of the drift and diffusion terms. The metastability, which is kinetic in origin, effectively suppresses the evolution of the size distribution on experimentally relevant time scales. However, thermodynamic equilibrium may eventually be approached over much longer time scales as a result of fluctuations in the array. Hence it is informative to compare the island size distributions we have obtained for metastable states with the predicted distributions at thermodynamic equilibrium. The distributions in the kinetic (metastable) and thermodynamic cases will not, in general, coincide since at a given temperature, a continuum of metastable states exist due to kinetics, whereas there is a unique distribution at thermodynamic equilibrium which minimizes the total array free energy.

A. Island size distribution at thermodynamic equilibrium

We have used the method of Ref. 26 to calculate the island size distribution at thermodynamic equilibrium. Under the constraint of a given total deposited quantity of material, the distribution at thermodynamic equilibrium $f_{eq}(N)$ is given by the Gibbs-Boltzmann formula Eq. (2). We here define $f_{eq}(N)dN$ as the concentration of islands per unit atomic site containing a number of atoms between N and $N+dN$. The distribution $f_{eq}(N)$ given by Eq. (2) is the steady-state solution of the Fokker-Planck evolution equation [Eqs. (9) and (6)] satisfying $J=0$.

At the temperature $T=0$, the distribution $f_{eq}(N)$ is infinitely sharp with its maximum at the optimum size $N=N_0$ (see Sec. IV). At finite temperature, the chemical potential of the system $\bar{\mu}$ is determined following Ref. 26 by the mass conservation requirement that the number of atoms deposited is equal to the total number of atoms within the islands:

$$q=\int_0^\infty Nf_{eq}(N)dN, \tag{33}$$

where q is the surface coverage. Once $\bar{\mu}$ is determined, the size distribution is obtained from Eq. (2). The resulting distribution as a function of size N depends on q, N_0, and T/Θ. It is independent of W.

For the calculation of the equilibrium size distribution, the choice of the value to use for N_0 was based upon the estimates for C_1 and C_2 given in Ref. 28 for InAs/GaAs(001) submonolayer islands. Hence the ratio $C_1/C_2=3.27$ was chosen, and substituting this ratio in Eq. (21) gives the $T=0$ optimum island size $N_0=5.1\times10^3$. Also we choose a small coverage $q=0.1$, consistent with our model of a sparse array (Sec. IV). Figure 10 shows the calculated size distribution $f_{eq}(N)$ at various temperatures. At low temperatures, as T/Θ is increased from $T=0$ in Fig. 10(a), the optimum island size N_{opt} at which the distribution peaks decreases from the value $N_{opt}=N_0$ at $T=0$. Accompanying this shift in N_{opt} is a broadening of the distribution with increasing temperature due to thermal fluctuations. As T/Θ is increased further in Fig. 10(b), the distribution continues to shift to smaller island sizes and broaden. By $T/\Theta=7.5\times10^{-3}$, the size N_{opt} at which the main distribution peaks has decreased below half

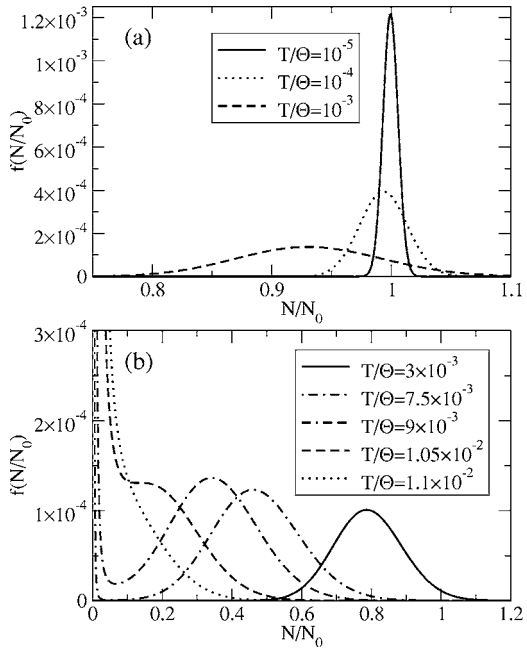

FIG. 10. Island size distribution at thermodynamic equilibrium for an array with coverage $q=0.1$ at various temperatures T/Θ. (a) Distribution at low values of T/Θ. (b) Distribution at high values of T/Θ. Here the value of the optimum island size at $T=0$ is $N_0=5.1\times10^3$.

TABLE II. Comparison of the width of the island size distribution at thermodynamic equilibrium for various temperatures T/Θ. The optimum island size N_{opt} and the full width at half maximum (FWHM) Δ_{eq} correspond to the calculated distributions at thermodynamic equilibrium from Fig. 10. The FWHM $\Delta_{anal}(N_{opt})$ corresponds to the analytical result obtained for a metastable state centered at N_{opt} using Eq. (29).

T/Θ	N_{opt}/N_0	$\frac{d\mu/dN\|_{N=N_{opt}}}{\varepsilon_0/N_0}$	Δ_{eq}/N_0	$\Delta_{anal}(N_{opt})/N_0$
10^{-5}	0.999	0.250	1.49×10^{-2}	1.49×10^{-2}
10^{-4}	0.993	0.252	4.69×10^{-2}	4.69×10^{-2}
10^{-3}	0.930	0.269	0.144	0.144
3×10^{-3}	0.787	0.315	0.230	0.230
7.5×10^{-3}	0.461	0.490	0.292	0.291
9×10^{-3}	0.342	0.580	0.296	0.293

its value N_0 at $T=0$. In addition, the distribution develops a bimodal characteristic with a second peak appearing at very small island sizes for individual adatoms. At higher temperatures we continue to denote by N_{opt} the optimum island size corresponding to the local maximum in the distribution at larger sizes (this peak corresponds to nanometer scale islands). As the temperature is increased further, N_{opt} continues to decrease until at $T/\Theta=1.05\times10^{-2}$ the local maximum for nanometer scale islands disappears. Above this temperature, the distribution decreases monotonically with island size.

B. Comparison with distributions in a metastable state

We can make a direct comparison between the distributions at thermodynamic equilibrium shown in Fig. 10 and the metastable distributions obtained earlier in this paper. The temperature range $T/\Theta=10^{-5}$ to $T/\Theta=7.5\times10^{-3}$ used in the simulations of Sec. V and Sec. VI B corresponds to the regime in Fig. 10 in which the peak for individual adatoms does not form a significant part of the distribution. Hence we concentrate on the main body of the distribution corresponding to nanoscale islands. The shapes of the distributions at thermodynamic equilibrium are very similar to those obtained in the metastable states (cf. Figs. 2, 4, and 7–9), being again Gaussian-like and quite symmetric. The trend for the increasing width of the distribution with temperature is also similar in both cases. At thermodynamic equilibrium, there is a unique optimum island size N_{opt} corresponding to the local maximum in the distribution for nanoscale islands. For metastable states, however, there exist a continuum of mean island sizes around which a distribution may be centered. The interesting comparison to make here is between the value for N_{opt} obtained for the thermodynamic distribution and the mean island size at which a metastable state is entered following evolution from sizes below N_1 (corresponding to the chemical potential minimum). This corresponds to the experimentally relevant case of evolution of islands from a small size following nucleation. A simulation of such evolution toward a metastable state was performed in Sec. V A at the temperature $T/\Theta=10^{-3}$. Despite the exponential slowing of the rate of evolution in that simulation, it is unlikely that the evolution has completely stopped by the final distribution reached in Fig. 2(b) (it was not possible to extend to later times due to computational constraints). However, the results suggest that a metastable state is entered at around $\bar{N}/N_0 \approx 0.3$. This is clearly well below the corresponding optimum size at thermodynamic equilibrium $N_{opt}/N_0=0.93$ from Fig. 10(a). Hence an array of islands within this metastable state would be able to reduce its free energy if it were able to grow to larger sizes. Such growth is likely to be kinetically suppressed by the metastable state, but fluctuations in the array could allow a slow drift in the direction of larger sizes. Consequently thermodynamic equilibrium may be approached experimentally over much longer time scales.

It is possible at a given temperature to compare quantitatively the width of the distribution at thermodynamic equilibrium with that in a metastable state located at the same mean island size. Since we saw in Sec. VI B that the analytical result of Eq. (29) gives an excellent approximation to the distribution width in a metastable state, we will use this expression in our comparison. Table II makes a detailed comparison between the observed distribution width Δ_{eq} at thermodynamic equilibrium in Fig. 10 and the predicted width Δ_{anal} from Eq. (29) in a metastable state centered at N_{opt}. Here the optimum island size N_{opt} corresponds to the local maximum for nanometer-scale islands taken from Fig. 10. It can be seen that the width at thermodynamic equilibrium is predicted remarkably well by Δ_{anal}. At all temperatures considered, Δ_{anal} matches the observed width to within about 1%. This is true even for $T/\Theta=9\times10^{-3}$, the highest temperature considered with a well defined value for N_{opt} from Fig. 10. This is despite the fact that at this temperature a significant fraction of the distribution lies at sizes below N_1, with a growing peak for individual adatoms. Hence the analytical expression for Δ_{anal} from Eq. (29) is equally applicable to predicting the width of size distributions at thermodynamic equilibrium and in metastable states. The reason for this is that Eq. (29) follows from imposing the condition $J=0$ and hence is valid for any steady-state solution, within the approximation of a linear chemical potential variation with island size (see Sec. VI A).

Note that the shape of the distribution in the metastable states obtained earlier in this paper using the kinetic method of Secs. II and III did not depend upon the coverage. Instead the coverage simply scales the absolute magnitude of the distribution [see Eq. (32)]. In contrast, the shape of the dis-

tribution at thermodynamic equilibrium does depend upon the coverage, although the dependence is very weak for low temperatures. The reason for this difference is that in the kinetic case, the mass conservation condition of Eq. (19) depends only on the flux (i.e., the rate of change of the coverage), rather than the absolute magnitude of the coverage. However, for the calculation at thermodynamic equilibrium, the coverage explicitly enters the mass conservation condition of Eq. (33).

VIII. DISCUSSION AND CONCLUSIONS

In this paper we have considered the evolution and stability of MEA systems, focusing on the illustrative system of 2D strained islands. Such islands exhibit a thermodynamically favored size at which the island energy per atom attains a minimum value. In addition, such islands also exhibit a minimum in the chemical potential with respect to island size. Island size distributions have been evolved in time numerically via a mean-field model using a Fokker-Planck equation. During annealing, we have shown that metastable states with a narrow size distribution naturally arise. The existence of these states depends only on the presence of a positive gradient in chemical potential with respect to island size. We have observed how the distribution width in a metastable state broadens with increasing temperature, and how the width is well described by an analytical expression obtained within the approximation of a linear chemical potential variation with island size. We have shown how this expression for the width also applies to the predicted island size distribution at thermodynamic equilibrium.

It is important to appreciate the significance of the metastable states considered in this paper in the context of nanostructure evolution. MEA systems are usually interpreted in terms of thermodynamic equilibrium.[14,16,39] However, our work illustrates that metastable states can arise before thermodynamic equilibrium is attained and so kinetic factors may determine experimentally observed size distributions during coarsening.

In this paper we have considered the evolution of MEA systems in the absence of a deposition flux (annealing). The incorporation of a nonzero deposition flux enables the possibility of tuning the mean size of the island size distribution in a metastable state.[17,18] In the presence of a small deposition flux, the distribution will be dominated by the metastable state at the current island size, but with a slight perturbation so that the islands slowly grow. This results in a gradual drift of the distribution to larger island sizes without any significant broadening.[18] By proceeding with the deposition for the required duration, the size distribution may be tuned to a desired mean island size before terminating the deposition. Hence the metastable distribution can be regarded as being tunable by the deposition flux.

The unusual behavior of a narrow size distribution which does not apparently broaden as the mean island size increases with deposition has recently been observed experimentally for metallic islands.[9] Such islands are thought to possess a minimum in chemical potential with respect to island size (i.e., regions of positive gradient)[15] and hence we expect metastable states to exist. The metastability considered in this paper could therefore explain the trends observed in this experiment.

An alternative strategy for controlling the island size distribution is a two-stage growth-anneal approach.[17] This strategy differs from that above in that a deposition flux of appreciable magnitude is incorporated during the growth phase so that the evolution is not metastable during this phase. By terminating the deposition at the desired mean island size, the distribution narrows into a metastable state.[17]

The existence of the narrow metastable distributions considered in this paper depends only upon the presence of a positive gradient in chemical potential with respect to island size. A wide range of material systems and island geometries may potentially possess such a characteristic. Shape transitions in MEA systems have also been modeled assuming thermodynamic equilibrium.[39] The analysis in this paper indicates that metastable states will have an important influence on the kinetics of the transition and in establishing the experimentally observed island size distributions.[40] Hence our results have important implications for nanostructure self-organization, shape transformations, and the fabrication of uniformly sized arrays with size selectivity.

ACKNOWLEDGMENTS

T.P.M. acknowledges a studentship provided by the EPSRC. D.E.J. acknowledges support from the ARC. V.A.Sh. and D.B. are grateful to the Deutsche Forschungsgemeinschaft (Sfb296) and the BMBF. Part of the work was supported by the SANDiE Network of Excellence of the European Commission, Contract Number NMP4-CT-2004-500101. V.A.Sh. acknowledges support from the Russian Foundation for Basic Research.

*On leave from A. F. Ioffe Physical Technical Institute, St. Petersburg 194021, Russia.

[1] D. Bimberg, M. Grundmann, and N. N. Ledentsov, *Quantum Dot Heterostructures* (Wiley, Chichester, 1998).

[2] V. A. Shchukin, N. N. Ledentsov, and D. Bimberg, *Epitaxy of Nanostructures* (Springer, Berlin, 2003).

[3] D. J. Eaglesham and M. Cerullo, Phys. Rev. Lett. **64**, 1943 (1990).

[4] D. Leonard, K. Pond, and P. M. Petroff, Phys. Rev. B **50**, 11687 (1994).

[5] J. M. Moison, F. Houzay, F. Barthe, L. Leprince, E. André, and O. Vatel, Appl. Phys. Lett. **64**, 196 (1994).

[6] N. P. Kobayashi, T. R. Ramachandran, P. Chen, and A. Madhukar, Appl. Phys. Lett. **68**, 3299 (1996).

[7] M. Valden, X. Lai, and D. W. Goodman, Science **281**, 1647 (1998).

[8] C. Xu, X. Lai, G. W. Zajac, and D. W. Goodman, Phys. Rev. B **56**, 13464 (1997).
[9] Z. Gai, B. Wu, J. P. Pierce, G. A. Farnan, D. Shu, M. Wang, Z. Zhang, and J. Shen, Phys. Rev. Lett. **89**, 235502 (2002).
[10] V. I. Marchenko, JETP Lett. **33**, 381 (1981).
[11] D. Vanderbilt, Surf. Sci. Lett. **268**, L300 (1992).
[12] K.-O. Ng and D. Vanderbilt, Phys. Rev. B **52**, 2177 (1995).
[13] C. Priester and M. Lannoo, Phys. Rev. Lett. **75**, 93 (1995).
[14] V. A. Shchukin, N. N. Ledentsov, P. S. Kop'ev, and D. Bimberg, Phys. Rev. Lett. **75**, 2968 (1995).
[15] F. Liu, Phys. Rev. Lett. **89**, 246105 (2002).
[16] I. Daruka and A.-L. Barabási, Phys. Rev. Lett. **79**, 3708 (1997).
[17] T. P. Munt, D. E. Jesson, V. A. Shchukin, and D. Bimberg, Appl. Phys. Lett. **85**, 1784 (2004).
[18] D. E. Jesson, T. P. Munt, V. A. Shchukin, and D. Bimberg, Phys. Rev. Lett. **92**, 115503 (2004).
[19] J. W. Christian, *The Theory of Transformations in Metals and Alloys*, 2nd edition (Pergamon Press, Oxford, 1975), Chap. 10, p. 418.
[20] E. M. Lifshitz and L. P. Pitaevskii, *Physical Kinetics* (Butterworth-Heinemann, Oxford, 1981).
[21] J. J. L. Velázquez, J. Stat. Phys. **92**, 195 (1998).
[22] H. A. Atwater and C. M. Yang, J. Appl. Phys. **67**, 6202 (1990).
[23] W. H. Press, S. A. Teukolsky, W. T. Vetterling, and B. P. Flannery, *Numerical Recipes in Fortran 77* (Cambridge University Press, Cambridge, 1992).
[24] J. F. Hawley, J. R. Wilson, and L. L. Smarr, Astrophys. J., Suppl. **55**, 211 (1984).
[25] We note that the average elastic interaction for a sparse array will modify the MEA volume (see Refs. 11–13). However, the MEA, chemical potential minimum and metastable states still persist for sparse arrays, even if the long-range interaction is taken into account.
[26] V. A. Shchukin, N. N. Ledentsov, and D. Bimberg, in *Self-Organized Processes in Semiconductor Alloys*, edited by A. Mascarenhas, D. Follstaedt, T. Suzuki, and B. Joyce, MRS Symposia Proceedings No. 583 (Materials Research Society, Pittsburgh, 2000), p. 23.
[27] V. A. Shchukin, N. N. Ledentsov, A. Hoffmann, D. Bimberg, I. P. Soshnikov, B. V. Volovik, V. M. Ustinov, D. Litvinov, and D. Gerthsen, Phys. Status Solidi B **224**, 503 (2001).
[28] V. A. Shchukin, N. N. Ledentsov, and D. Bimberg, in *Atomistic Aspects of Epitaxial Growth*, edited by M. Kotrla, I. Papanicolaou, D. D. Vvedensky, and L. T. Wille, NATO Science Series, Series II: Mathematics, Physics and Chemistry (Plenum, New York, 2002), Vol. 65, p. 397.
[29] D. E. Jesson, Transactions of the Royal Society of South Africa **58**, 141 (2003).
[30] V. A. Shchukin and D. Bimberg, Rev. Mod. Phys. **71**, 1125 (1999).
[31] Actually, this optimum island size N_0 obtained by the minimization of the energy per atom only applies at the temperature $T=0$. At finite temperature, the relevant quantity to minimize is the Helmholtz free energy, $F \equiv E - TS$, where S is the entropy and all quantities are defined per atom.
[32] F. M. Ross, J. Tersoff, and R. M. Tromp, Phys. Rev. Lett. **80**, 984 (1998).
[33] W. Theis, N. C. Bartelt, and R. M. Tromp, Phys. Rev. Lett. **75**, 3328 (1995).
[34] N. C. Bartelt, W. Theis, and R. M. Tromp, Phys. Rev. B **54**, 11741 (1996).
[35] The factor $N^{1/2}$ arises because the length of the island perimeter (which determines the number of sites available for adatom attachment/detachment) scales according to this factor for 2D islands.
[36] F. Liu, A. H. Li, and M. G. Lagally, Phys. Rev. Lett. **87**, 126103 (2001).
[37] Recall that in a drift-dominant regime, $\bar{\mu}$ is a weighted mean of $\mu(N)$ over $f(N,t)$.
[38] By $t/\tau = 2.7 \times 10^{-2}$, we find $\partial f(N,t)/\partial t = 0$ within the numerical precision of the calculation. However, there is no noticeable change in $f(N,t)$ beyond $t/\tau = 1.1 \times 10^{-2}$.
[39] G. Medeiros-Ribeiro, A. M. Bratkovski, T. I. Kamins, D. A. A. Ohlberg, and R. S. Williams, Science **279**, 353 (1998).
[40] D. J. Vine, D. E. Jesson, M. J. Morgan, V. A. Shchukin, and D. Bimberg, Phys. Rev. B **72**, 241304(R) (2005).